

# A Chimeric Peptide Logic Gate for Orthogonal Stimuli-Triggered Precise Tumor Therapy

Xinxin Dai, Kai Han,\* Zhaoyu Ma, and Heyou Han\*

The precise recognition of tumor tissue is the key challenge that hinders successful clinical translation of drug delivery systems. Herein, a tumor extracellular matrix orthogonal stimuli-responsive chimeric peptide is developed for logic gate controlled tumor recognition and photodynamic therapy. In vitro studies show that the negatively charged chimeric peptide is sensitive to two typical tumor hallmarks, i.e., mild acidity and matrix metalloproteinase 2 (MMP-2) simultaneously. Consequently, the chimeric peptide can undergo charge reversal from negative charge to positive charge in tumor, accelerating the cellular uptake. Specifically, the enhanced cellular uptake of chimeric peptide can be activated efficiently only in the presence of both acidity and MMP-2, endowing chimeric peptide with highly specific tumor therapy both in vitro and in vivo. This chimeric peptide based “AND” logic gate should show great potential in precise tumor therapy.

## 1. Introduction

Drug delivery systems (DDSs) have received increasing attention in tumor therapy during last decades.<sup>[1,2]</sup> Various nanomaterials including liposomes, polymers, and inorganic nanoparticles have been engineered for DDSs.<sup>[3–5]</sup> Although DDSs can passively accumulate in tumor tissue via enhanced penetration and retention (EPR) effect, the further development of DDSs is remarkably retarded owing to the poor tumor accumulation efficacy.<sup>[6]</sup> To overcome this hurdle, DDSs have been modified with bioresponsive groups. Usually, these bioresponsive groups can respond with tumor microenvironments including enzymes or mild acidity to endow DDSs with tumor active target and improved therapeutic efficacy.<sup>[7,8]</sup> In our previous study, we reported a tumor acidity responsive chimeric peptide for tumor tissue/nuclei-targeted photodynamic therapy.<sup>[9]</sup> Zhang et al. reported multifunctional envelope-type mesoporous silica nanoparticles for matrix metalloproteinase-triggered tumor-targeted drug delivery.<sup>[10]</sup> Many DDSs respond to the single stimulus

in tumor tissue/cells. However, thus far most tumor target individual biomarker is also shared, at least to some degree, by other tissues.<sup>[11,12]</sup> As a result, DDSs will be nonspecific uptake by normal tissue/cells during in vivo circulation. Besides, many biofunctional linkages including acidity-responsive hydrazone bond or enzyme-responsive ester bond are not stable enough, exposing the tumor recognition motif in DDSs in advance.<sup>[13]</sup> All these issues will make single stimulus responsive DDSs mistake the normal tissue for tumor tissue and induce adverse off-target effects.


Nowadays, logic gate nanoplatfoms exhibit great potential in nanomedicine.<sup>[14–16]</sup> It is well established that logic gate DDSs can respond to multiple stimuli

in tumor tissue/cells, realizing tumor specific drug delivery and release. However, a fairly large number of logic gates are “OR” type, but not “AND” type, endowing that these multiple stimuli responsive DDSs can be activated by just single stimulus. While in the “AND” logic gate DDSs, many DDSs respond to the tumor extracellular and intracellular stimuli in a cascade manner, restricting their application in controlled drug release, but not tumor recognition. It can be imagined that if the “AND” logic gate DDSs could respond to multiple stimuli in the same site in a simultaneous way, a precise tumor strike could be expected.

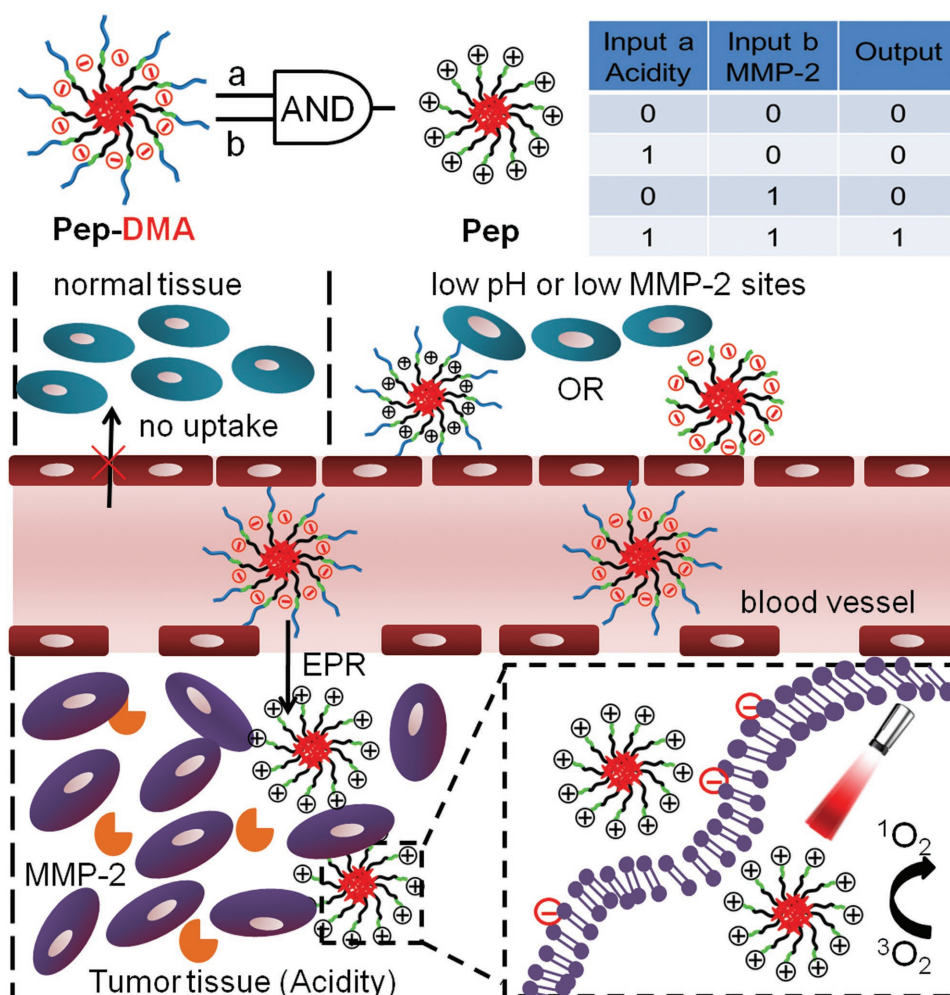
Keeping all these issues in mind, we develop a simple but rational chimeric peptide (protoporphyrin-Ahx-K<sub>8</sub>(DMA)-PLGVR-PEG<sub>8</sub>, designated as Pep-DMA) as the effective pH “AND” enzyme logic gate to display tumor precise photodynamic therapy. As shown in **Scheme 1**, amphiphilic Pep-DMA could self-assemble into spherical nanoparticles. Due to the existence of polyethylene glycol (PEG) and dimethyl maleic anhydride (DMA) groups, Pep-DMA self-assembly was negatively charged in normal physiological environment, endowing Pep-DMA to resist with protein absorption and non-specific cellular uptake during circulation. It is anticipated that pH sensitive DMA group can be detached under tumor mild acidity, while PLGVR sequence can be hydrolyzed by overexpressed matrix metalloproteinase 2 (MMP-2) in tumor, liberating PEG sequence. However, peptide self-assembly will not suffer from negative-to-positive charge reversal under either the detachment of DMA group or PEG sequence alone (Figure S1, Supporting Information). Charge reversal-mediated cellular uptake of chimeric peptide only occurs in tumor tissue upon cleavage of the PLGVR sequence (in the presence of MMP-2) AND detachment of DMA group (at low pH) in a simultaneous manner.

X. X. Dai, Prof. K. Han, Z. Y. Ma, Prof. H. Y. Han  
State Key Laboratory of Agricultural Microbiology  
College of Science  
Huazhong Agricultural University  
Wuhan 430070, China  
E-mail: hank@mail.hzau.edu.cn; hyhan@mail.hzau.edu.cn

X. X. Dai, Prof. K. Han, Prof. H. Y. Han  
Bio-Medical Center  
Huazhong Agricultural University  
Wuhan 430070, China

 The ORCID identification number(s) for the author(s) of this article can be found under <https://doi.org/10.1002/adfm.201804609>.

DOI: 10.1002/adfm.201804609



**Scheme 1.** Illustration of logic gate controlled drug delivery of Pep-DMA under orthogonal stimuli for precise photodynamic therapy in tumor.

## 2. Results and Discussion

### 2.1. Synthesis and Characterization of Pep-DMA

To construct the chimeric peptide logic gate, protoporphyrin-Ahx-K<sub>8</sub>-PLGVR-PEG<sub>8</sub> was synthesized by the standard N-fluorenyl-9-methoxycarbonyl (Fmoc) solid-phase peptide synthesis (SPPS) method.<sup>[17]</sup> Electrospray ionization mass spectrometry and high performance liquid chromatography confirmed the validity and purity of peptide (Figure S2A,B, Supporting Information). Then DMA was modified on peptide under alkaline environment to obtain Pep-DMA (<sup>1</sup>H NMR spectrum shown in Figure S3, Supporting Information). Pep-DMA showed good water solubility as validated by the UV-vis spectrum (Figure 1A). Free protoporphyrin (PpIX) had a significantly broadened split Soret band with two peaks at 361 and 450 nm,<sup>[18,19]</sup> while Pep-DMA showed a peak

around 400 nm, demonstrating the little aggregation in Pep-DMA. Meanwhile, UV-vis spectrum of Pep-DMA still kept stable and Pep-DMA showed well solubility, when Pep-DMA was lyophilized and then redissolved in water, suggesting the

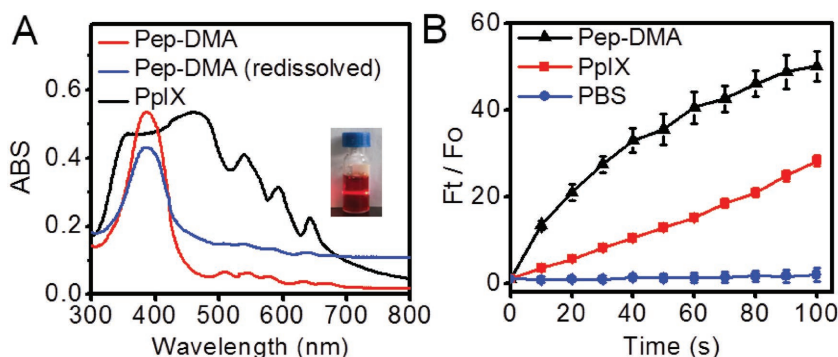


**Figure 1.** A) UV-vis spectrum of Pep-DMA, PpIX in water, and redissolved Pep-DMA after lyophilization (inset was the image of redissolved Pep-DMA with a laser irradiation). B) ROS generation of Pep-DMA under light irradiation using DCFH-DA as the sensor. Both PpIX and 0.1% DMSO and PBS were used as controls. Data are presented as mean  $\pm$  S.D. ( $n = 3$ ).

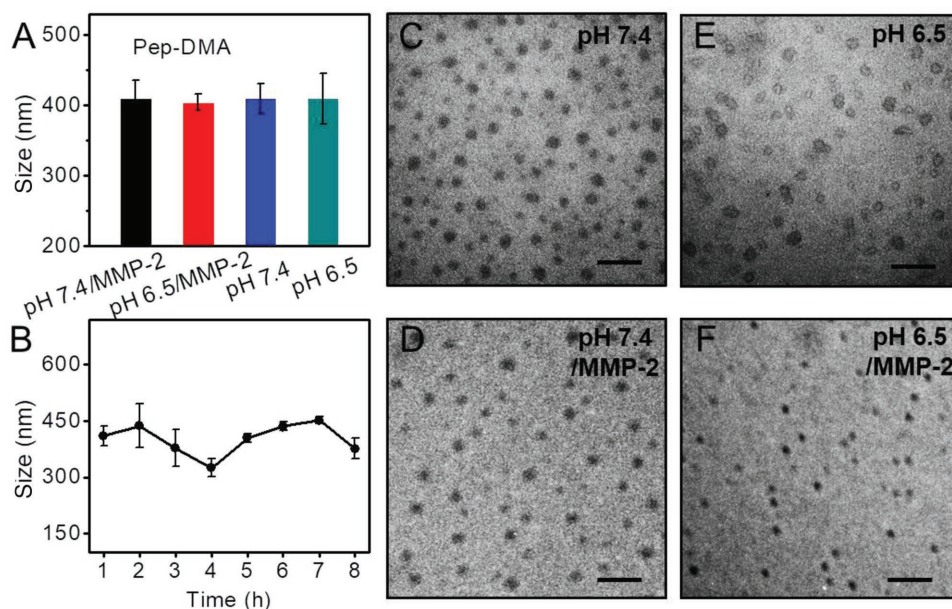


**Figure 2.** A) Hydrodynamic size of Pep-DMA at pH 6.5 and 7.4 in the presence or absence of MMP-2. B) Pep-DMA stability in PBS as a function of time. Data are presented as mean  $\pm$  S.D. ( $n = 3$ ). TEM images of Pep-DMA at pH 7.4 in the C) absence and D) presence of MMP-2. TEM images of Pep-DMA at pH 6.5 in the E) absence and F) presence of MMP-2. Scale bar: 100 nm.

well storage ability and potential clinical application. When free photosensitizer got irradiated with appropriate wavelength, it would be excited to triplet state, participating in a one electron oxidation–reduction reaction with a neighboring molecule to form radical intermediates. These radical intermediates react with oxygen to generate reactive oxygen species (ROS). The good water solubility of Pep-DMA facilitated the efficient ROS generation. 2',7'-dichlorodifluorescein diacetate (DCFH-DA) that can be rapidly oxidized to green fluorescence DCF was employed as a ROS sensor.<sup>[20,21]</sup> As shown in Figure 1B, almost no change in fluorescence was detected in phosphate buffer solution (PBS) group. For free PpIX in 0.1% dimethyl sulfoxide (DMSO), a relatively lower fluorescence increment was observed due to the self-quenching among aggregated PpIX. By contrast, the fluorescence intensity of DCF in Pep-DMA group increased significantly, suggesting the improved water solubility of PpIX in Pep-DMA increased ROS generation. It is crucial for photodynamic therapy, since ROS can kill tumor cells through oxidation of biological molecules including proteins and nucleic acids.

Dynamic light scattering results verified that Pep-DMA showed a size around 400 nm, regardless of pH change from 7.4 to 6.5 and the existence of MMP-2 (Figure 2A). Meanwhile, Pep-DMA was highly stable in PBS buffer (Figure 2B). Transmission electron microscope (TEM) image exhibited that Pep-DMA self-assembled into spherical nanoparticles of uniform size at pH 7.4 (Figure 2C) and pH 6.5 (Figure 2E), and the existence of MMP-2 did not change the self-assembly behavior remarkably (Figure 2D,F).

## 2.2. Orthogonal Stimuli-Triggered Charge Reversal of Pep-DMA

To verify the orthogonal stimuli responsive property of Pep-DMA, zeta potential changes under different pHs and/or in presence of

MMP-2 were measured. MMP-2 insensitive PpIX-Ahx-K<sub>8</sub>(DMA)-LPVGG-PEG<sub>8</sub> (denoted as C-Pep-DMA) and acidity-insensitive PpIX-Ahx-K<sub>8</sub>(succinic anhydride)-PLGVR-PEG<sub>8</sub> (denoted as Pep-SA) were used as the controls. As shown in Figure 3A, in the absence of MMP-2, the zeta potential of Pep-DMA increased to some extent at pH 6.5. While at pH 7.4 this change was not significant. Clearly, the detachment of acidity sensitive DMA could expose the positively charged amino group in Lys.<sup>[22]</sup> However, the electroneutral PEG sequence was still at the out shell of nanoparticles (Figure S1, Supporting Information), restricting the further increase of surface charge.<sup>[23]</sup> For comparison, in the presence of MMP-2, the zeta potential of Pep-DMA also exhibited limited increase at pH 7.4, since MMP-2 could hydrolyze PLGVR sequence and the high instability of dimethylmaleic amide leads to the increased zeta potential. Note that Pep-DMA was still negatively charged under just single stimulus, which would avoid nonspecific cellular uptake. Interestingly, the zeta potential of Pep-DMA changed from  $-31.0$  to  $9.7$  mV at pH 6.5 in the presence of MMP-2. Undoubtedly, the simultaneous orthogonal stimuli of acidity and MMP-2 could thoroughly liberate Lys, resulting in the negative-to-positive charge reversal of chimeric peptide. Besides, the zeta potential of C-Pep-DMA changed from  $-38$  to  $-18$  mV at pH 6.5 regardless of the existence of MMP-2 (Figure 3B). Since MMP-2 could not cleave the LPVGG sequence and PEG sequence would be reserved at the out shell. For Pep-SA, zeta potential only slightly increased from around  $-32.0$  to  $-28.0$  mV at 4 h ignoring pH changes or the enzyme existence (Figure 3C). Since the terminal carboxyl group was far away from succinic amide in Pep-SA, which could not assist the hydrolysis of succinic amide.

To further detect the acid-labile property, DMA detachment from Pep-DMA was studied using fluorescamine as a probe. Fluorescamine is unfluorescent, but it can quickly react with primary amine to emit strong fluorescence.<sup>[24,25]</sup> As shown in

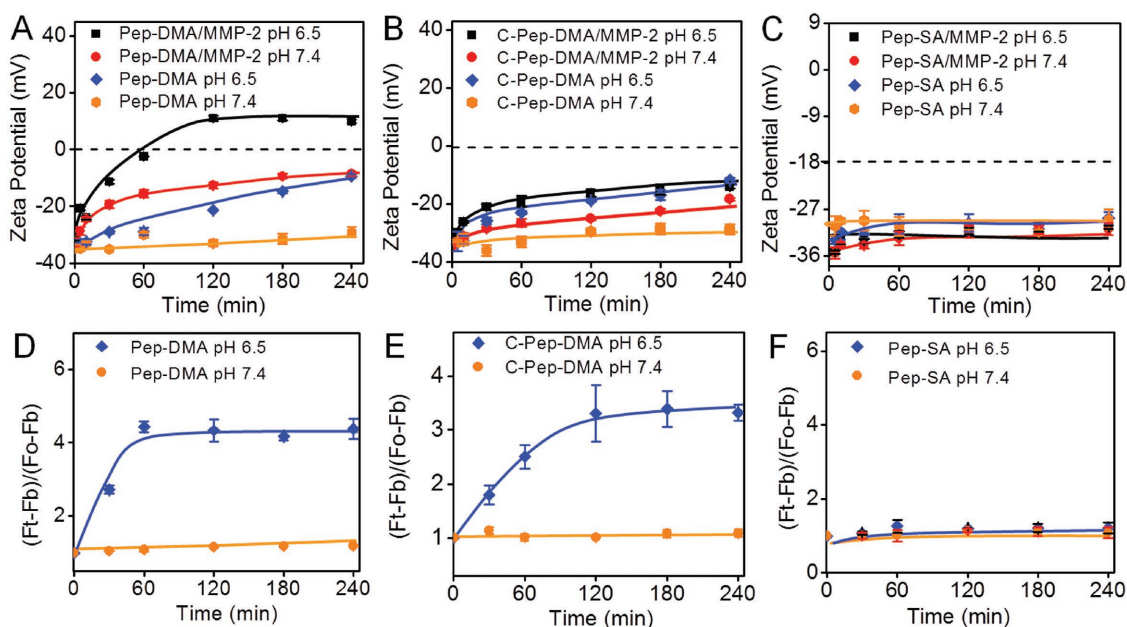


**Figure 3.** A) Zeta potential changes of Pep-DMA at pH 6.5 and 7.4 in the presence or absence of MMP-2. B) Zeta potential changes of C-Pep-DMA at pH 6.5 and 7.4 in the presence or absence of MMP-2. C) Zeta potential changes of Pep-SA at pH 6.5 and 7.4 in the presence or absence of MMP-2. Detachment of DMA group from D) Pep-DMA, E) C-Pep-DMA, and F) Pep-SA at pH 6.5 and 7.4, respectively. Fluorescamine was used as the sensor. Data are presented as mean  $\pm$  S.D. ( $n = 3$ ).

Figure 3D,E, after 4 h incubation, the fluorescence increment of Pep-DMA at pH 6.5 was significantly greater than that at pH 7.4 (Figure 3D), and it rapidly reached a platform within 1 h at pH 6.5, since low acidity detached DMA group exposed primary amine in lysine and then reacted rapidly with the fluorescamine. Similar result was also found for pH sensitive C-Pep-DMA (Figure 3E). By sharp contrast, the fluorescence of Pep-SA kept stable regardless of pH change (Figure 3F) due to the acidic stability of Pep-SA.

### 2.3. Orthogonal Stimuli-Activated Tumor Specific Cellular Uptake of Pep-DMA

It is well documented that pH in normal tissue is around 7.4, while the pH in tumor is slightly acidic ranging from 6.3 to 6.9.<sup>[26,27]</sup> Meanwhile, tumor extracellular matrix is rich in MMP-2.<sup>[28]</sup> It is expected that after Pep-DMA reached the tumor area, the charge reversal behavior will benefit the tumor cell internalization through the electrostatic effect, lighting tumor cells due to the fluorescent PpIX inside cells. To confirm it, the cellular uptakes of various samples in SCC-7 (squamous cell carcinoma, high expression of MMP-2) or COS7 (African green monkey SV40-transfected kidney fibroblast cells, normal cells with negligible expression of MMP-2) cells were observed via confocal laser scanning microscopy (CLSM). In SCC-7 cells, the fluorescence intensity of Pep-DMA in the presence of MMP-2 at pH 6.5 (Figure 4A1) was remarkably higher than that of Pep-DMA in the absence of MMP-2 at pH 6.5 (Figure 4A2) or Pep-DMA in the presence of MMP-2 at pH 7.4 (Figure 4A3). These results were consistent with that of zeta potential. Apparently, the simultaneous orthogonal stimuli of

acidity and MMP-2 activated the charge reversal of chimeric peptide, leading to enhanced cellular internalization. The single stimulus would not liberate cationic amino group in Lys completely, i.e., shielded by negatively charged DMA group (just in presence of MMP-2) or neutrally charged PEG sequence (just at pH 6.5), which could significantly retard the cellular uptake of chimeric peptide. Besides, cellular uptake of Pep-DMA in human cervical carcinoma cell (HeLa cells, another MMP-2-positive tumor cells) was also provided in Figure S4 (Supporting Information), similar results were observed when compared with that in SCC-7 cells, confirming its tumor-selectivity.

For comparison, C-Pep-DMA showed low fluorescence at pH 6.5 in presence of MMP-2 in SCC-7 cells (Figure 4B1), which was much weaker than that of Pep-DMA at pH 6.5 in SCC-7 cells. And the fluorescence of C-Pep-DMA at pH 6.5 in the presence or absence of MMP-2 (Figure 4B1,B2) was just slightly higher than that at pH 7.4 in the presence of MMP-2 (Figure 4B3). In addition, Pep-SA could not be taken up by SCC-7 cells in the presence or absence of MMP-2 at pHs of 6.5 and 7.4 (Figure 4C1–C3). C-Pep-DMA and Pep-SA exhibited the size around 376.1 and 300 nm, respectively (Figure S5, Supporting Information), which were comparable to the size of Pep-DMA, suggesting size would not contribute the difference. Clearly, the improved cellular internalization of Pep-DMA was due to the presence of orthogonal-stimuli of low pH and MMP-2. Weak fluorescence of Pep-DMA was observed in COS7 cells at pHs of 6.5 and 7.4 (Figure 4D1,D2), suggesting the tumor-specific cellular uptake of Pep-DMA.

Furthermore, flow cytometry was used to determine the cellular uptake quantitatively. The choice of flow cytometry gate was based on the principle that the blank control cells should be totally negative. As shown in Figure 5, Pep-DMA positive

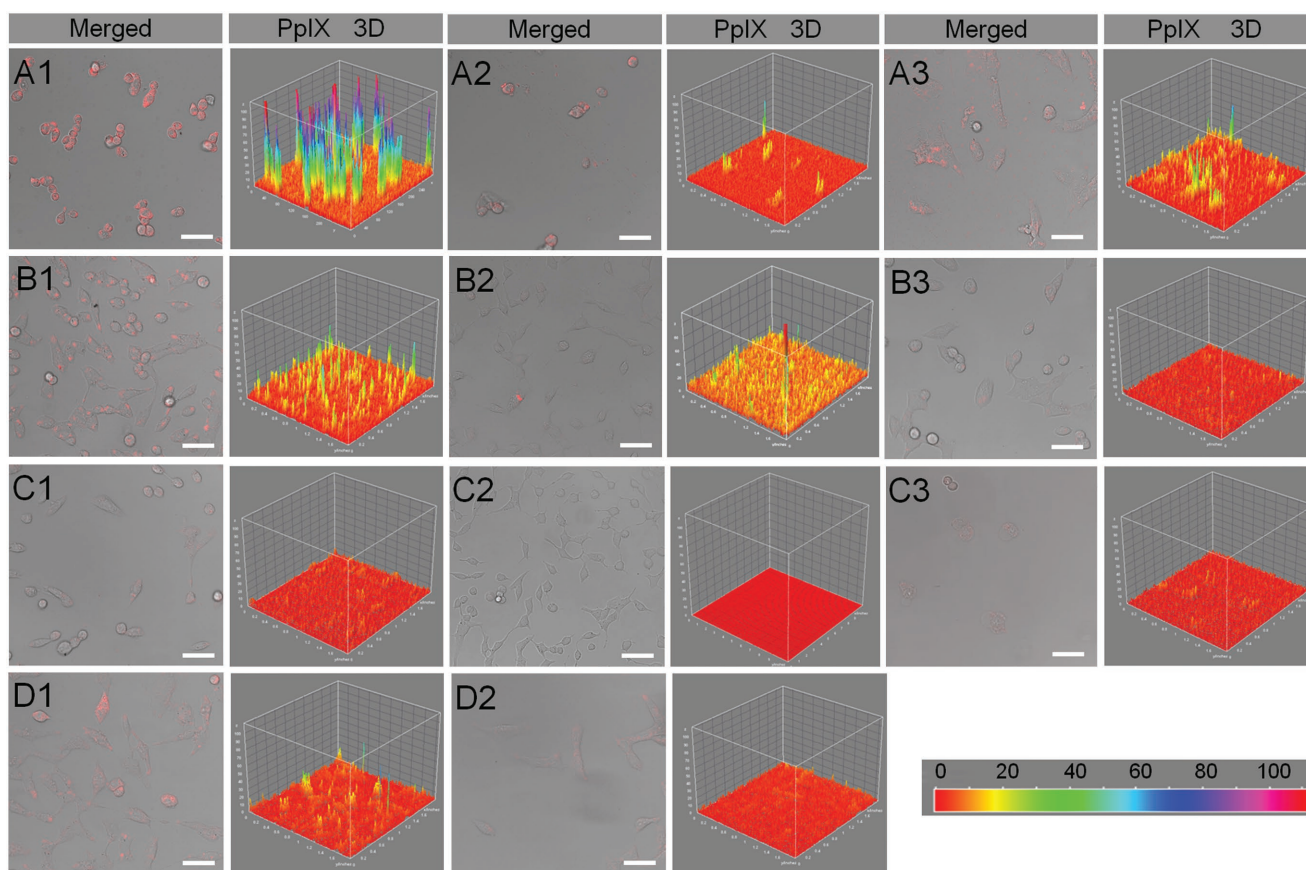


**Figure 4.** Cellular internalization observation via CLSM: Pep-DMA at pH 6.5 in SCC-7 cells in the A1) presence or A2) absence of MMP-2. A3) Pep-DMA at pH 7.4 in SCC-7 cells in the presence of MMP-2. C-Pep-DMA in SCC-7 cells at pH 6.5 in the B1) presence or B2) absence of MMP-2. B3) C-Pep-DMA at pH 7.4 in SCC-7 cells in the presence of MMP-2. Pep-SA in SCC-7 cells at pH 6.5 in the C1) presence or C2) absence of MMP-2. C3) Pep-SA at pH 7.4 in SCC-7 cells in the presence of MMP-2; Pep-DMA in COS7 cells at D1) pH 6.5 and D2) pH 7.4, respectively. Merged means the overlay of bright field of cells and fluorescence of PpIX. Scale bar: 50  $\mu\text{m}$ .

SCC-7 cells reached 47.3% in the presence of pH 6.5 and MMP-2 (Figure 5D), which was over threefold than that only in the presence of MMP-2 (14.7%, Figure 5B) or pH 6.5 (15.6%, Figure 5C). For comparison, C-Pep-DMA positive SCC-7 at pH 6.5 in the presence or absence of MMP-2 was slightly higher than that at pH 7.4 in presence of MMP-2 (Figure 5E–G). Besides, Pep-SA exhibited no difference in cellular uptake in SCC-7 cells among pH 7.4 with MMP-2, pH 6.5 in the presence or absence of MMP-2, Pep-SA positive SCC-7 cells were negligible (Figure 5H–J). Similarly, Pep-DMA positive COS7 at pH 6.5 was also slightly higher than that at pH 7.4 (Figure 5L,M), suggesting that the acidity-triggered detachment of DMA could not significantly enhance the cellular uptake. All these results had a similar tendency with that of CLSM. Flow cytometry experiments were conducted for three times and the average data were provided in Figure 5N.

#### 2.4. Precise Photodynamic Therapy In Vitro

Although free PpIX could not recognize tumor cells (Figure S6, Supporting Information), the logic gate controlled tumor specific uptake of Pep-DMA should realize precise toxicity against

tumor cells while not damaging the normal cells. To confirm it, methyl thiazolyl tetrazolium (MTT) assay was employed. Pep-DMA exhibited good biocompatibility in COS7 cells even with light irradiation. The cell viability difference between pH 6.5 and 7.4 was only 16% (PpIX concentration:  $0.8 \text{ mg L}^{-1}$ ) (Figure 6A). It was due to the fact that the expression of MMP-2 was negligible in COS7 cells, so Pep-DMA could not suffer from the charge reversal, leading to very limited toxicity in COS7 cells at pH 6.5. By sharp contrast, for Pep-DMA in SCC-7 cells with abundant MMP-2, the difference in toxicity between pH 6.5 and 7.4 reached 50% when PpIX concentration was  $0.8 \text{ mg L}^{-1}$ , and only around 25% cells lived at pH 6.5 (Figure 6B). Apparently, both the existence of acidity and MMP-2 dramatically elevated the cell damage efficacy and realized the tumor specific photodynamic therapy. Subsequently, the toxicity of C-Pep-DMA against SCC-7 cells was also investigated. Figure 6C revealed that the toxicity difference in toxicity between pH 6.5 and pH 7.4 was very limited, since MMP-2 in SCC-7 cells could not hydrolyze LPVGG sequence in C-Pep-DMA,<sup>[29]</sup> the reserved PEG sequence restricted the cellular uptake of chimeric peptide as well as phototoxicity. Besides, acidity insensitive Pep-SA exhibited negligible toxicity due to the electrostatic repulsion between Pep-SA and cell membrane (Figure 6D). In addition, Pep-DMA caused no damage in

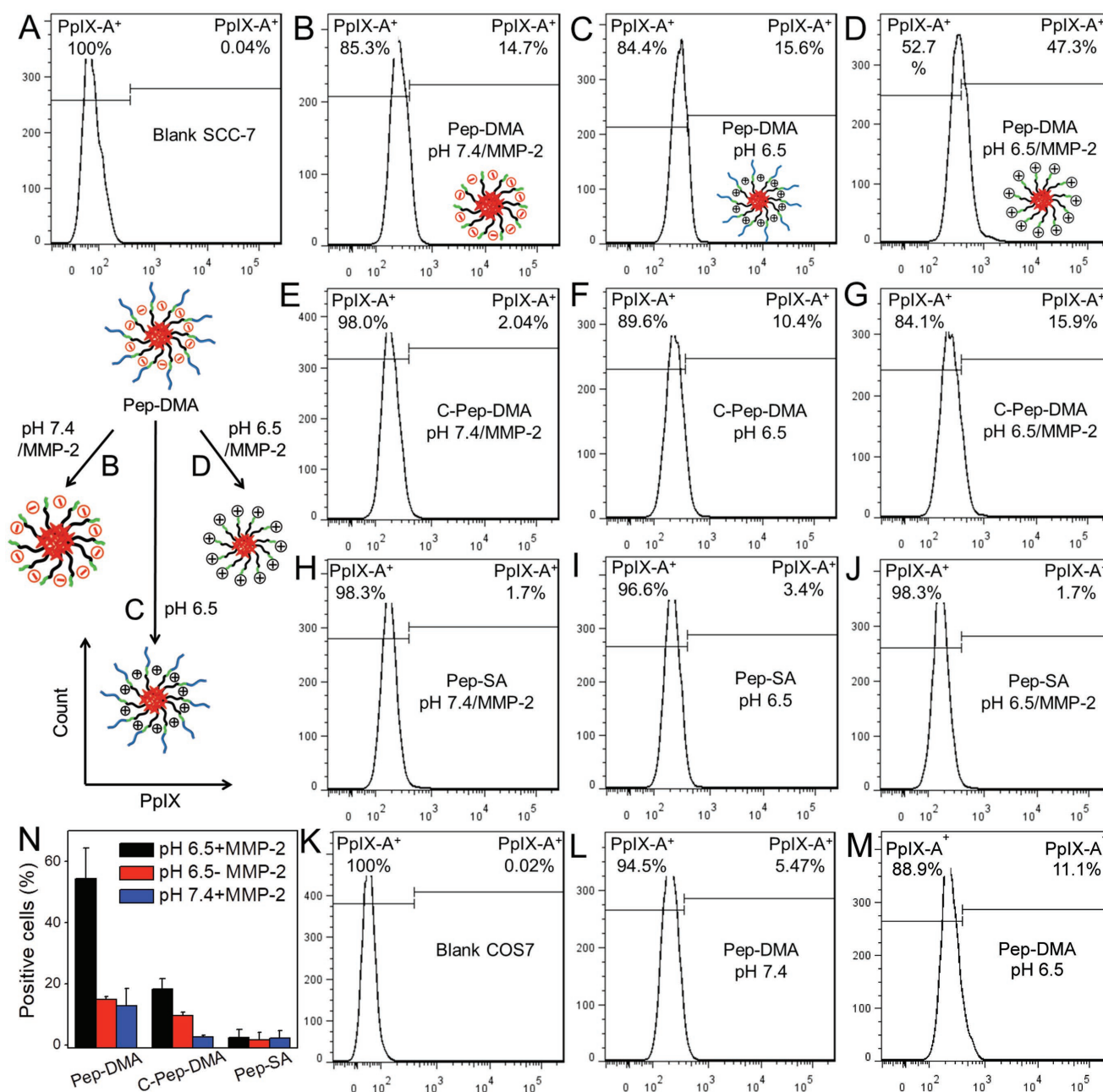


**Figure 5.** Flow cytometry analysis of the internalization of various samples in cells: A) blank SCC-7 cells; B) Pep-DMA at pH 7.4 in SCC-7 cells in the presence of MMP-2; Pep-DMA at pH 6.5 in SCC-7 cells in the C) absence or D) presence of MMP-2. E) C-Pep-DMA at pH 7.4 in SCC-7 cells in the presence of MMP-2; C-Pep-DMA at pH 6.5 in SCC-7 cells in the F) absence or G) presence of MMP-2. H) Pep-SA in SCC-7 cells at pH 7.4 in SCC-7 cells in the presence of MMP-2; Pep-SA at pH 6.5 in SCC-7 cells in the I) absence or J) presence of MMP-2. K) Blank COS7 cells; Pep-DMA in COS7 cells at L) pH 7.4 and M) pH 6.5, respectively. N) The average positive cells of various samples via flow cytometry. Data are presented as mean  $\pm$  S.D. ( $n = 3$ ).

SCC-7 cells without light irradiation even in the presence of both acidity and MMP-2 (Figure S7, Supporting Information), suggesting the excellent biocompatibility of Pep-DMA.

To directly visualize the potent, tumor specific phototoxicity of Pep-DMA under the orthogonal stimuli of acidity and MMP-2, calcein AM, and iodinated pyridine (PI) staining were employed.<sup>[30,31]</sup> According to the protocol, the cell viability can be reflected via the ratio of red/green fluorescence. As shown in Figure 7A2, SCC-7 cells incubated with Pep-DMA

clearly showed greatest cell deaths at pH 6.5 in the presence of MMP-2. The numbers of red dots were significantly higher than that at pH 6.5 in the absence of MMP-2 (Figure 7A1) or that at pH 7.4 in the presence of MMP-2 (Figure 7A3). For comparison, the groups of C-Pep-DMA (Figure 7B1,B2) and Pep-SA (Figure 7C1,C2) in SCC-7 cells at pH of 6.5 or 7.4 in the presence of MMP-2 showed few red dots. Similar results were also found in the group of Pep-DMA at pH of 6.5 or 7.4 in the absence of MMP-2 (Figure 7D1,D2) in COS7 cells. All

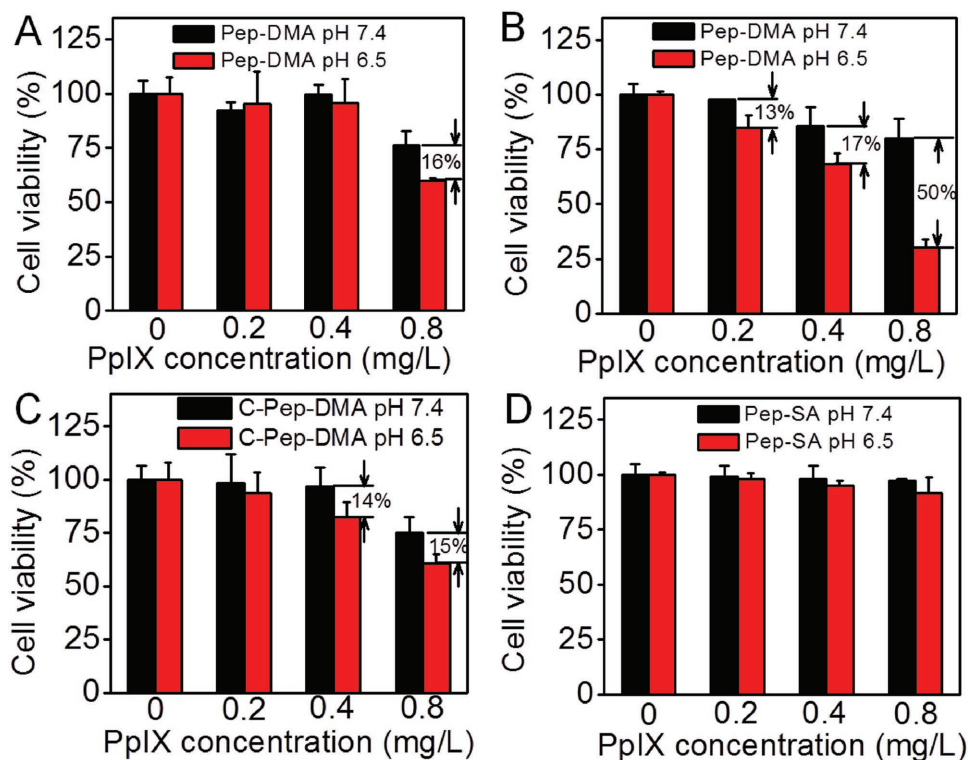


**Figure 6.** In vitro cytotoxicity of A) Pep-DMA in COS7 cells; B) Pep-DMA in SCC-7 cells; C) C-Pep-DMA in SCC-7 cells; D) Pep-SA in SCC-7 cells at pHs of 6.5 and 7.4. Data are presented as mean  $\pm$  S.D. ( $n = 8$ ).

these results demonstrated that the damage of Pep-DMA to cells strongly depended on the simultaneous existence of tumor hallmarks acidity and MMP-2. Single stimulus would not activate the phototoxicity, ensuring the high specificity of Pep-DMA to tumor cells.

Furthermore, the apoptosis behaviors mediated by various samples were observed via CLSM using Annexin V-FITC/PI as the sensors. When cell undergoes early apoptosis, phosphatidylserine (PS) turns from the inner side to the outer side of the cell membrane. Annexin V-FITC can specifically bind the extracellular exposed PS and reveal the early apoptotic cells.<sup>[32,33]</sup> As shown in Figure S8A2 (Supporting Information), SCC-7 cells incubated with Pep-DMA with the existence of MMP-2 and acidity exhibited strong green and red fluorescence, and these two fluorescents were overlapped in most of cells, indicating that SCC-7 cells were in the stage of metaphase and late apoptosis.<sup>[34]</sup> By contrast, Pep-DMA induced a small amount of cell death at pH 6.5 in the absence of MMP-2, only a few green and red fluorescence cells were observed (Figure S8A1, Supporting Information). Meanwhile, almost no fluorescence was apparent at pH 7.4 in the presence of MMP-2 for Pep-DMA (Figure S8A3, Supporting Information), suggesting that at pH 7.4 Pep-DMA could not damage cells. For comparison, C-Pep-DMA (Figure S8B1,B2, Supporting Information) and Pep-SA (Figure S8C1,C2, Supporting Information) showed negligible fluorescence in the presence of MMP-2 regardless of pH change. Similarly, the group of Pep-DMA in COS7 cells showed extremely weak fluorescence at pH of 6.5 or 7.4 (Figure S8D1,D2, Supporting Information). These results were

in line with the above results, suggesting the logic gate based chimeric peptide realize high specificity in tumor therapy. This chimeric peptide logical gate demonstrated here is different from our previous acidity responsive work.<sup>[35]</sup> Our previous work utilized tumor acidity alone to trigger the intramolecular fold of peptide, leading to pop up of shielded tumor target ligand to the surface of nanoparticles for accelerated accumulation in tumor. It represented a steric shielding protected/tumor acidity-activated strategy for tumor targeted therapy. While in this work, pH “AND” enzyme logic gate was used for tumor precise photodynamic therapy.

### 2.5. Precise Photodynamic Therapy In Vivo with Minimal Side Effects

Subsequently, in vivo tumor target of various samples was observed via small animal imaging system. H22 tumor-bearing mouse, but not the SCC-7 tumor-bearing mouse, was used as the animal model, since the SCC-7 cells were originated from human, SCC-7 tumor was hard to establish in mouse. However, H22 tumor grew rapidly in mice and also expressed high level of MMP-2. Samples were injected intravenously. As shown in Figure 8A, the fluorescence of Pep-DMA in tumor region kept stable due to the EPR effect, while the fluorescence of C-Pep-DMA and Pep-SA in tumor region gradually decreased with time. At 24 h postinjection, the organs and tumors were imaged (Figure 8B). It was found that the fluorescence in tumor of Pep-DMA was significantly higher than that

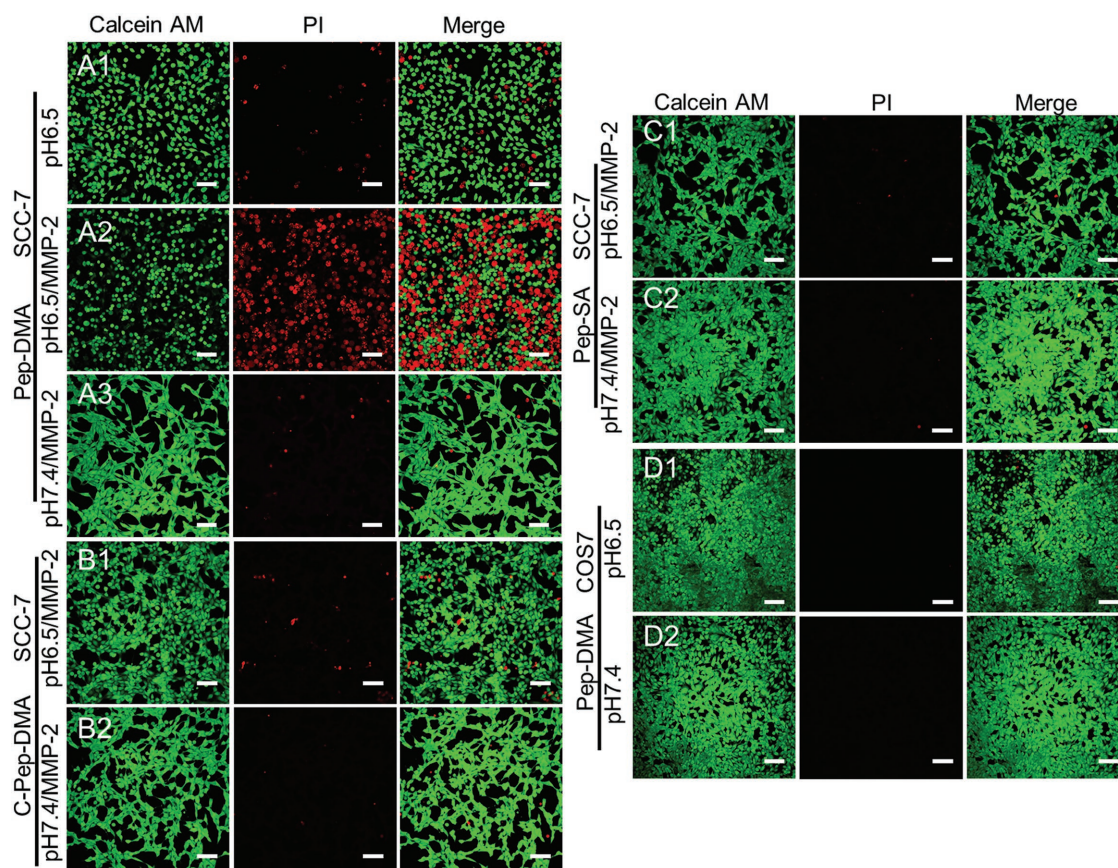


**Figure 7.** Calcein AM/PI staining: Pep-DMA in SCC-7 cells A1) at pH 6.5 in absence of MMP-2; A2) at pH 6.5 in presence of MMP-2 and A3) at pH 7.4 in presence of MMP-2. C-Pep-DMA in SCC-7 cells B1) at pH 6.5 in presence of MMP-2 and B2) at pH 7.4 in presence of MMP-2. Pep-SA in SCC-7 cells C1) at pH 6.5 in presence of MMP-2 and C2) at pH 7.4 in presence of MMP-2. Pep-DMA in COS7 cells D1) at pH 6.5 and D2) at pH 7.4. Green signal: live cells; Red signal: dead cells. Scale bar: 75  $\mu\text{m}$ .

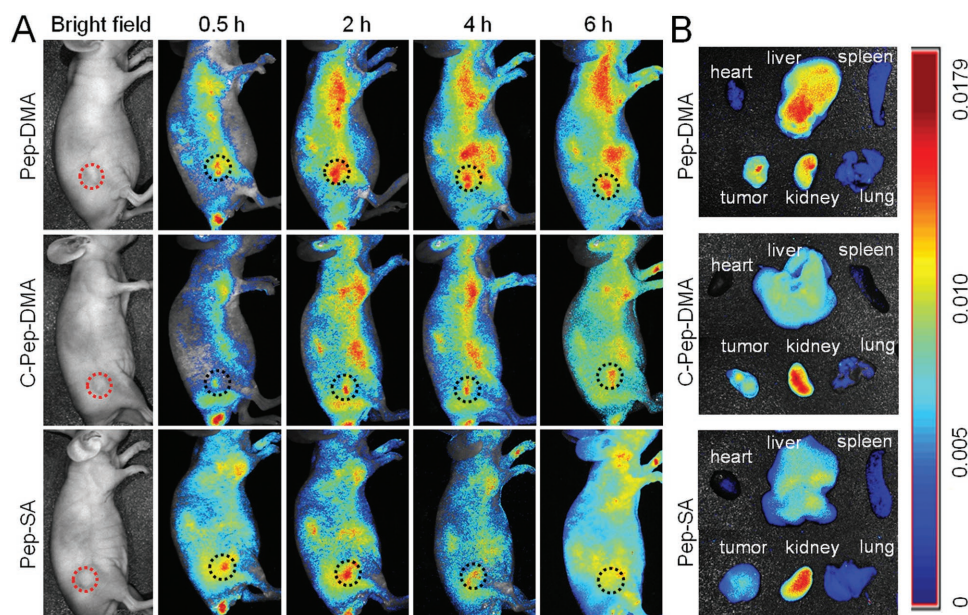


**Figure 8.** A) The in vivo fluorescence imaging of various samples at different time points: 0, 0.5, 2, 4, 6 h. B) The fluorescence images of organs and tumors in various samples at 24 h postinjection.



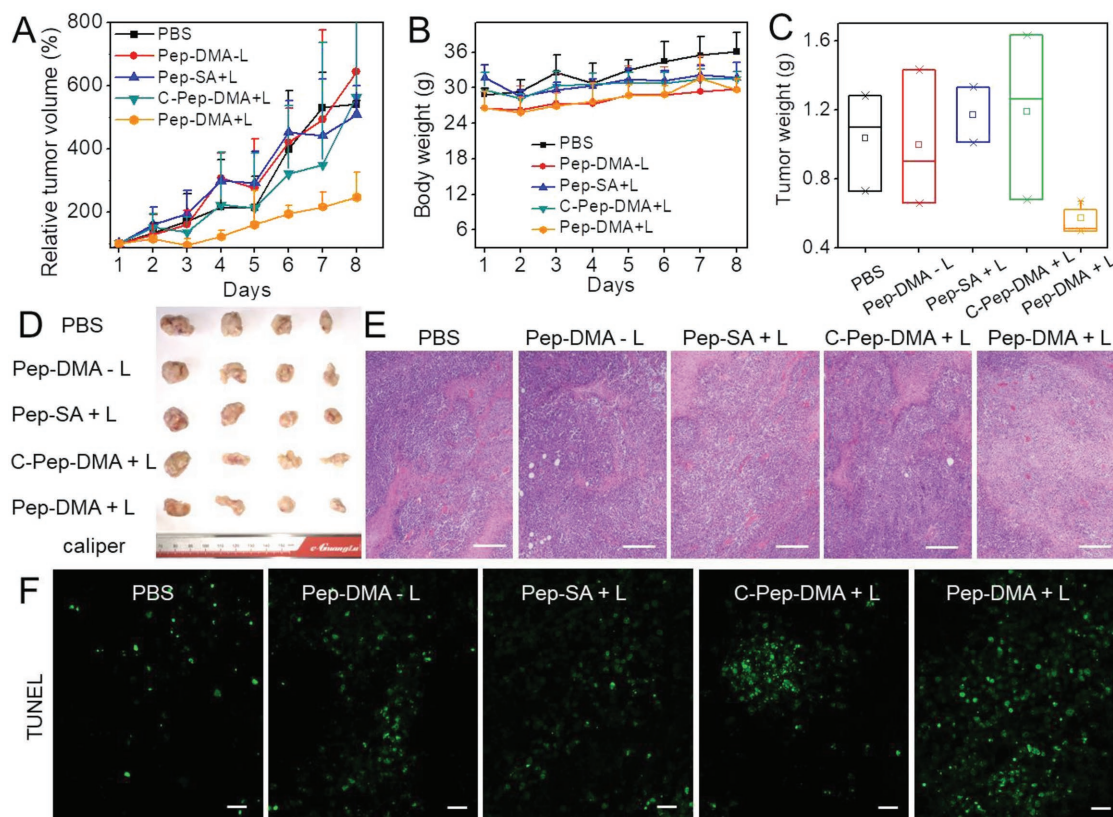


**Figure 9.** A) Relative tumor volume curves during the treatment, samples were injected every day (PpIX concentration:  $3 \text{ mg kg}^{-1}$  mouse body weight). B) Body weights change during the treatment. C) Tumor weights after the mice were sacrificed. D) Tumor images of various groups. E) H&E staining ( $40\times$ , scale bar:  $200 \mu\text{m}$ ) and F) TUNEL staining ( $40\times$ , scale bar:  $50 \mu\text{m}$ ) of tumors in various groups, green dots meant dead cells. L: light irradiation.

of C-Pep-DMA and Pep-SA, indicating the better accumulation and target of Pep-DMA in tumor. Note that obvious Pep-DMA signal was observed in both liver and kidney, while C-Pep-DMA and Pep-SA were mainly found in the kidney, since kidney and liver were the main metabolic organs, leading to the nonspecific kidney and liver uptake. Meanwhile, although the sizes were comparable, Pep-DMA has the larger size (Figure 2A; Figure S5, Supporting Information), preferring to accumulation in liver. The relative mean fluorescence intensity in tumor was also performed in Figure S9 (Supporting Information).

Furthermore, the mice were injected with samples and the tumor volume was measured by a caliper. It was found that the tumors in control groups including Pep-SA with light irradiation, Pep-DMA without light irradiation, and C-Pep-DMA with light irradiation showed rather rapid growth, which were even similar to the PBS group (Figure 9A). The tumor growth speed could only be delayed if the mice were injected with Pep-DMA with light irradiation. During the treatment, the body weight of mice slightly increased in all groups (Figure 9B). After the mice were executed, the tumors were weighed up. Figure 9C showed that the tumors in Pep-DMA group with light irradiation were significantly smaller than other groups. The stripped tumors in various groups were also exhibited in Figure 9D. Clearly, Pep-DMA performed the most efficient tumor inhibition after photodynamic therapy. It was most probably due to the orthogonal stimuli-triggered charge reversal of Pep-DMA, which enhanced the cellular internalization, tumor

accumulation, and subsequent photodynamic therapeutic efficacy in tumor. Besides, the hemotoxylin and eosin (H&E) staining (Figure 9E) and terminal-deoxynucleotidyl transferase mediated nick end labeling (TUNEL, Figure 9F) further demonstrated the improved therapeutic efficacy of Pep-DMA with light irradiation, when compared with other groups.

To evaluate the potential toxicity, complete blood panel test was conducted. As shown in Figure 10, all measured parameters including white blood cell (WBC), red blood cell (RBC), hemoglobin (Hb), packed-cell volume (PCV), mean corpuscular volume (MCV), mean corpuscular hemoglobin (MCH), mean corpuscular hemoglobin concentration (MCHC), eosinophil (%), basophil (%), variation coefficient of erythrocyte distribution (RDW-CV), standard deviation of the distribution of red blood cells (RDW-SD), and thrombocytocrit (PCT) fell within normal ranges,<sup>[36]</sup> indicating that photodynamic therapy with Pep-DMA should be well tolerable by those mice. On the other hand, the physiological morphology of various organs was also observed via H&E staining. Figure S10 (Supporting Information) showed that not significant pathological lesion was found in all tissues, suggesting the negligible side effects during the in vivo treatment.

### 3. Conclusion

In summary, we developed a tumor extracellular matrix responsive amphipathic peptide Pep-DMA and realized logic gate

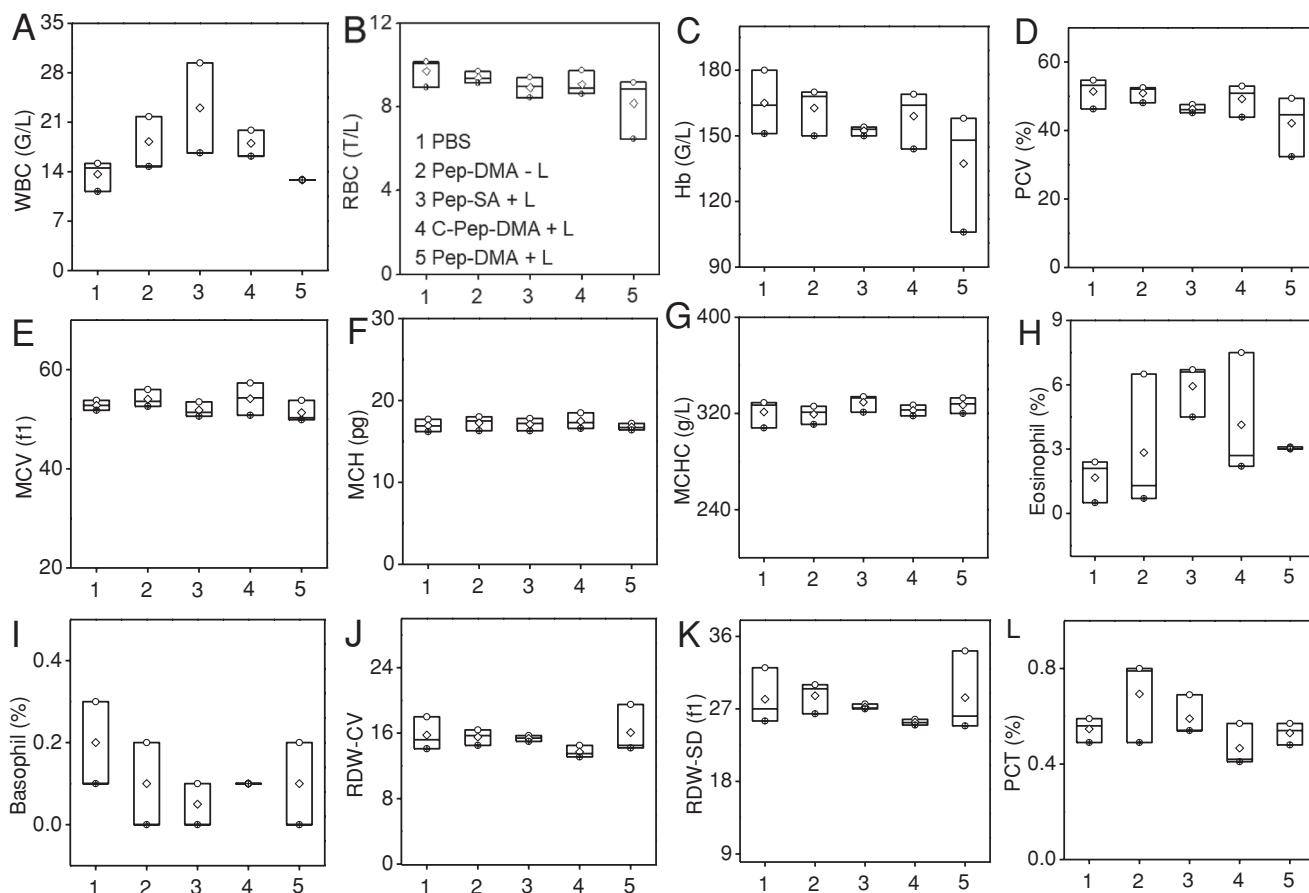


**Figure 10.** The complete blood test of various samples: A) WBC; B) RBC; C) Hb; D) PCV; E) MCV; F) MCH; G) MCHC; H) eosinophil (%); I) basophil (%); J) RDW-CV; K) RDW-SD; L) PCT. L: light irradiation. Data are presented as mean  $\pm$  S.D. ( $n = 3$ ).

controlled, tumor specific internalization and photodynamic therapy. Under the orthogonal stimuli, i.e., acidity and MMP-2, in tumor tissue, Pep-DMA underwent the surface charge reversal, resulting in tumor enhanced cellular uptake. While a single stimulus, either acidity or MMP-2, would not activate the charge reversal process as well as tumor internalization, which dramatically elevate the therapeutic accuracy. Different from many “AND” or “OR” logic gate systems that nanocarriers respond to different stimuli in different regions via a cascade manner, our chimeric peptide based logic gate responded to the orthogonal stimuli in the same site (tumor extracellular matrix) via a simultaneous way, which precisely manipulated the cellular uptake behavior of drug. This strategy should show great potential for precise tumor therapy.

#### 4. Experimental Section

**Materials:** 2-chlorotriethyl chloride resin (loading:  $0.9 \text{ mmol g}^{-1}$ ), Fmoc-protected L-amino acids, diisopropylethylamine, and o-benzotriazole- $N,N,N',N'$ -tetramethyluroniumhexa fluorophosphate piperidine were bought from GL Biochem Ltd. (Shanghai, China). Fluorescamine and Fmoc-Ahx-COOH were provided by Sigma-Aldrich (USA). Succinic anhydride (SA) from sinopharm (Beijing, China) and DMA from Aladdin (Shanghai, China) were obtained. Trifluoroacetic acid and triisopropylsilane were obtained from Shanghai Reagent Chemical

Co. (China). Trypsin, dulbecco's modified Eagle's medium (DMEM), streptomycin, penicillin, fetal bovine serum (FBS), and MTT were purchased from GIBCO Invitrogen Corp.

**Synthesis of Pep-DMA and C-Pep-DMA:** Peptide was prepared via SPPS method as our previous report.<sup>[9]</sup> DMA was linked with peptide as previous report.<sup>[37]</sup> Peptide (5 mg) and 40 equiv. (to amino group) of DMA were dissolved in pure water. Then  $2 \text{ mol L}^{-1}$  NaOH was added drop-wise to make the pH around 10. After 24 h reaction in dark, the solution was dialyzed against water (molecular weight cut off (MWCO) 1000 Da). The obtained Pep-DMA and C-Pep-DMA were kept at  $4^\circ \text{C}$  for further use. The synthesis of Pep-SA was similar to that of Pep-DMA. UV-vis spectrum of Pep-DMA was collected by using a Lambda Bio40 spectrophotometer (PerkinElmer). Free PpIX (in 0.1% DMSO) was used as a control. The hydrodynamic size was measured by Nano-ZS ZEN3600 (Malvern Instruments) at  $25^\circ \text{C}$  in PBS. Pep-SA and C-Pep-DMA were used as controls. Morphology of Pep-DMA nanoparticles ( $50 \text{ mg L}^{-1}$ ) at different pHs of 6.5 and 7.4 with or without MMP-2 was observed by TEM (HITACHI H-7650 microscope).

**Singlet Oxygen Detection:** The ROS generation was measured via fluorescence spectrum. DCFH-DA was used as the sensor. DCFH-DA ( $30 \mu\text{L}$ ) was pretreated with NaOH and then Pep-DMA ( $50 \mu\text{L}$ ,  $100 \text{ mg L}^{-1}$ ) was added. At preset times, the fluorescence curves were recorded (Ex:  $485 \text{ nm}$ ) after irradiation. The ROS generation ability was calculated as  $F_t/F_0$ .  $F_0$  was the initial fluorescence with NaOH pretreated DCFH-DA alone. PpIX with equal amount (in 0.1% DMSO) was used as a negative control.

**Orthogonal Stimuli Response of Pep-DMA:** Pep-DMA was dissolved in PBS with different pHs of 6.5 and 7.4, respectively. Zeta potential of the solution was measured for 4 h. To test the zeta potential change in

presence of MMP-2, Pep-DMA was added to PBS buffer, and then quickly mixed with MMP-2, the corresponding zeta potential was measured.

**Amino Exposure:** Pep-DMA was dissolved in  $10 \times 10^{-3}$  M PBS buffer at pHs of 6.5 and 7.4. Then fluorescamine solution in DMF (2 mg mL<sup>-1</sup>, 0.2 mL) was added to all samples (1 mL), the solution was further incubated for 10 min at 37 °C. Thereafter, the fluorescence intensity ( $F_t$ ) was tested via a fluoro-spectrophotometer (Ex: 390 nm, Ex: 485 nm). When fluorescamine was added to Pep-DMA, the fluorescence was detected as soon as possible, which was defined as  $F_o$ , while  $F_b$  was defined as the fluorescence of PBS control. The degradation rate of DMA was calculated as following:  $(F_t - F_b)/(F_o - F_b)$ .

**Cellular Uptake Study:** The cellular uptake of chimeric peptide was observed via CLSM and flow cytometry. For CLSM observation, cells were seeded in the plates in DMEM with 10% FBS at pHs of 7.4 or 6.5 and incubated for 24 h. Then different samples (PpIX: 0.8 mg L<sup>-1</sup>) were added to the plates. After 4 h, the medium was removed and cells were washed with PBS for 5 times. Samples were observed via CLSM (Leica TCS SP8, German). For flow cytometry, SCC-7 cells and COS7 cells were seeded in six-well plates in DMEM with 10% FBS at pHs of 7.4 or 6.5 and incubated for 24 h, respectively. Then different samples (PpIX: 0.8 mg L<sup>-1</sup>) were added to the plates. After 4 h, the medium was removed. Then cells were washed with PBS for 5 times, digested with trypsin, and collected. Samples were quantified via a FACS Calibur flow cytometer (BC FC500, USA). Data were analyzed via Flow J software.

**Cytotoxicity In Vitro:** Cells were seeded on 96-well plates with a density of 6000 cells per well. 24 h later, the medium was removed and Pep-DMA nanoparticles with various concentrations at pHs of 7.4 or 6.5 (in DMEM with 10% FBS) were added. After incubation for 4 h, the medium was removed and 200  $\mu$ L fresh medium (pH 7.4) was added to each well. Cells received 45 s light irradiation (630 nm, 10 mW cm<sup>-2</sup>) and then further incubated for 24 h. Thereafter, MTT was added. 4 h later, the supernatant was replaced with DMSO (150  $\mu$ L). The optical density (OD) at 570 nm was determined via a microplate reader (PerkinElmer, 1420-032, USA). The relative cell viability was defined as following: cell viability (%) =  $OD_{(sample)}/OD_{(control)} \times 100\%$ .  $OD_{(sample)}$  was the OD value in the presence of sample, while  $OD_{(control)}$  was the OD value in the absence of sample. Pep-SA and C-Pep-DMA were employed as the controls.

**Calcein AM/PI Staining:** Cells were seeded in plates and incubated for 24 h. Then medium was not changed to avoid the removing of MMP-2, various samples (PpIX: 0.8 mg L<sup>-1</sup>) were added. SCC-7 cells and COS7 cells were incubated with various samples for 4 h, respectively. Then cells were washed with PBS buffer and received light irradiation for 45 s. Cells were further incubated for 24 h, and then stained with dyes (Calcein AM:  $1 \times 10^{-6}$  M; PI:  $4.5 \times 10^{-6}$  M). After 30 min, samples were observed via CLSM (Leica TCS SP8, German). For Pep-DMA at pH 6.5 in the absence of MMP-2, the culture medium in cells was replaced with fresh medium to remove the secreted MMP-2 and then Pep-DMA was added for the following experiments.

**Annexin V-FITC/PI Staining:** Cells were seeded in the plates at different pHs and incubated for 24 h. Then medium was not changed, Pep-DMA, Pep-SA, and C-Pep-DMA (PpIX: 1 mg L<sup>-1</sup>) were added into the plates, respectively. Cells were incubated with various samples for 4 h, then the medium was changed with fresh DMEM with 10% FBS and received light irradiation for 80 s. After further incubation for 24 h, the cells were washed with PBS for three times. Cells were finally incubated in binding buffer (400  $\mu$ L), and stained with Annexin V-FITC/PI dye (Annexin V-FITC : 5  $\mu$ L; PI : 10  $\mu$ L). After 30 min, samples were observed via CLSM. For Pep-DMA at pH 6.5 in the absence of MMP-2, the culture medium in cells was replaced with fresh medium to remove the secreted MMP-2 and then Pep-DMA was added for the following Annexin V-FITC/PI staining.

**In Vivo Fluorescence Imaging, Tissue Distribution:** H22 cells were injected into the back of female Kunming mice. When the volume of H22 tumor reached around 50 mm<sup>3</sup>, samples were injected through tail vein. The equivalent PpIX dosage of each formulation was 3 mg kg<sup>-1</sup>. The fluorescence imaging at the preset times and the tissue distribution at 24 h postinjection were obtained via a small animal imaging system (Institute of Virology, Chinese Academy of Sciences).

**In Vivo Antitumor Test and Toxicity Evaluation:** H22 tumor-bearing mice were divided into 5 groups (each group had 4 mice). The mice were intravenously injected with various samples, respectively (PpIX concentration: 3 mg kg<sup>-1</sup> mouse body weight). 6 h later, the mice injected with Pep-DMA, Pep-SA, and C-Pep-DMA received light irradiation (laser wavelength 638 nm, power density: 0.2 W cm<sup>-2</sup>, 10 min). The light irradiation performed on the tumor region. Tumor volume was recorded every day. When the treatment finished, mice blood was collected for whole blood analysis. Then mice were sacrificed and the main organs and tumor were collected for H&E and TUNEL staining.

## Supporting Information

Supporting Information is available from the Wiley Online Library or from the author.

## Acknowledgements

X.X.D. and K.H. contributed equally to this work. This work was financially supported by National Natural Science Foundation of China (Grant Nos. 51603080, 21375043, and 21778020), Fundamental Research Funds for the Central Universities (Grant No. 2662015QD026), National Key Research Development Program of China (Grant No. 2016YFD0500700), and Sci-tech Innovation Foundation of Huazhong Agricultural University (Grant No. 2662018PY024).

## Conflict of Interest

The authors declare no conflict of interest.

## Keywords

chimeric peptides, logic gate, orthogonal stimuli, tumor microenvironment, tumor targets

Received: July 5, 2018  
Revised: September 12, 2018  
Published online:

- [1] J. J. Shi, P. W. Kantoff, R. Wooster, O. C. Farokhzad, *Nat. Rev. Cancer* **2017**, *17*, 20.
- [2] M. Gaber, W. Medhat, M. Hany, N. Saher, J. Y. Fang, *J. Controlled Release* **2017**, *254*, 75.
- [3] D. Ruth, *Nat. Rev. Drug Discovery* **2003**, *2*, 347.
- [4] J. I. Harea, T. Lammers, M. B. Ashford, S. Puri, G. Storm, S. T. Barry, *Adv. Drug Delivery Rev.* **2017**, *108*, 25.
- [5] S. Vandghanooni, M. Eskandani, J. Barara, Y. Omid, *Eur. J. Pharm. Sci.* **2018**, *117*, 301.
- [6] K. Nazila, Z. Y. Xiao, M. V. Pedro, F. R.-M. Aleksandar, C. F. Omid, *Chem. Soc. Rev.* **2012**, *41*, 2971.
- [7] L. Wang, M. Huo, Y. Chen, J. Shi, *Adv. Healthcare Mater.* **2018**, *7*, 1701156.
- [8] T. Ji, J. Liang, J. Wang, R. Cai, Y. Zhang, F. Qi, L. Zhang, X. Zhao, W. J. Wu, J. H. Hao, Z. H. Qin, Y. Zhao, G. J. Nie, *ACS Nano* **2017**, *11*, 8668.
- [9] K. Han, W. Y. Zhang, J. Zhang, Q. Lei, S. B. Wang, J. W. Liu, X. Z. Zhang, H. Y. Han, *Adv. Funct. Mater.* **2016**, *26*, 4351.
- [10] J. Zhang, Z. F. Yuan, Y. Wang, W. H. Chen, G. F. Luo, S. X. Cheng, R. X. Zhuo, X. Z. Zhang, *J. Am. Chem. Soc.* **2013**, *135*, 5068.

- [11] B. A. Badeau, M. P. Comerford, C. K. Arakawa, J. A. Shadish, C. A. DeForest, *Nat. Chem.* **2018**, *10*, 251.
- [12] L. J. McCawley, L. Matrisian, *Mol. Med. Today* **2000**, *6*, 149.
- [13] E. Yuba, A. Yamaguchi, Y. Yoshizaki, A. Harada, K. Kono, *Biomaterials* **2017**, *120*, 32.
- [14] A. C. Evans, N. N. Thadani, J. Suh, *J. Controlled Release* **2016**, *240*, 387.
- [15] C. Angell, M. Kai, S. Xie, X. Dong, Y. Chen, *Adv. Healthcare Mater.* **2018**, *7*, 1701189.
- [16] J. Zhu, Y. Niu, Y. Li, Y. Gong, H. Shi, Q. Huo, Y. Liu, Q. Xu, *J. Mater. Chem. B* **2017**, *5*, 1339.
- [17] B. F. Green, L. N. Richard, *Chem. Biol. Drug Des.* **1990**, *35*, 161.
- [18] L. M. Scolaro, M. Castriciano, A. Romeo, S. Patanè, E. Cefalì, E. Allegrini, *J. Phys. Chem. B* **2002**, *106*, 2453.
- [19] G. F. Luo, W. H. Chen, S. Hong, Q. Cheng, W. X. Qiu, X. Z. Zhang, *Adv. Funct. Mater.* **2017**, *27*, 1702122.
- [20] G. Simbula, A. Columbano, G. M. Ledda-Columbano, L. Sanna, M. Deidda, A. Diana, M. Pibiri, *Apoptosis* **2007**, *12*, 113.
- [21] O. Tomoko, M. Atsushi, M. Akira, K. Shosuke, I. Tetsuro, T. Shigeru, *FEBS Lett.* **2002**, *511*, 21.
- [22] L. H. Liu, W. X. Qiu, Y. H. Zhang, B. Li, C. Zhang, F. Gao, L. Zhang, X. Z. Zhang, *Adv. Funct. Mater.* **2017**, *27*, 1700220.
- [23] Y. Bae, K. Kataoka, *Adv. Drug Delivery Rev.* **2009**, *61*, 768.
- [24] S. Udenfriend, S. Stein, P. Böhlen, W. Dairman, W. Leimgruber, M. Weigele, *Science* **1972**, *178*, 871.
- [25] J. R. Benson, P. E. Hare, *Proc. Natl. Acad. Sci. USA* **1975**, *72*, 619.
- [26] T. Ramasamy, H. B. Ruttala, B. Gupta, B. K. Poudel, H. G. Choi, C. S. Yong, J. O. Kim, *J. Controlled Release* **2017**, *258*, 226.
- [27] S. Peppicelli, F. Bianchini, L. Calorini, *Cancer Metastasis Rev.* **2014**, *33*, 823.
- [28] L. Brannon-Peppas, J. O. Blanchette, *Adv. Drug Delivery Rev.* **2012**, *64*, 206.
- [29] V. Knäuper, H. Wil, L. O. Carlos, B. Smith, S. J. Atkinson, H. Stanton, R. M. Hembry, G. Murphy, *J. Biol. Chem.* **1996**, *271*, 17124.
- [30] X. Zhang, C. Wang, J. Wu, Y. Liu, Z. Yang, Y. Zhang, X. Sui, M. Li, M. Feng, *J. Controlled Release* **2017**, *262*, 305.
- [31] Z. Y. Ma, K. Han, X. X. Dai, H. Y. Han, *ACS Nano* **2018**, *12*, 6252.
- [32] S. J. Martin, C. P. Reutelingsperger, A. J. McGahon, J. A. Rader, R. C. van Schie, D. M. LaFace, D. R. Green, *J. Exp. Med.* **1995**, *182*, 1545.
- [33] V. A. Fadok, A. de Cathelineau, D. L. Daleke, P. M. Henson, D. L. Bratton, *J. Biol. Chem.* **2001**, *276*, 1071.
- [34] J. Y. Lee, C. Crake, B. Teo, D. Carugo, M. de Saint Victor, A. Seth, E. Stride, *Adv. Healthcare Mater.* **2017**, *6*, 1601246.
- [35] K. Han, Z. Y. Ma, X. X. Dai, J. Zhang, H. Y. Han, *J. Controlled Release* **2018**, *279*, 198.
- [36] Q. Chen, L. Xu, C. Liang, C. Wang, R. Peng, Z. Liu, *Nat. Commun.* **2016**, *7*, 13193.
- [37] M. Y. Peng, D. W. Zheng, S. B. Wang, S. X. Cheng, X. Z. Zhang, *ACS Appl. Mater. Interfaces* **2017**, *9*, 13965.